Turbidity maximum zone index: A novel model for remote extraction of turbidity maximum zone in different estuaries

Chongyang Wang[1‡], Li Wang[1‡], Danni Wang[2], Dan Li[1,3], Chenghu Zhou[1,3,4], Hao Jiang[1,3], Qiong Zheng[1], Shuisen Chen[1], Kai Jia[1], Yangxiaoyue Liu[1,3], Ji Yang[1,3], Xia Zhou[1] and Yong Li[1,3]

[1] Guangdong Open Laboratory of Geospatial Information Technology and Application, Key Lab of Guangdong for Utilization of Remote Sensing and Geographical Information System, Guangzhou Institute of Geography, Guangdong Academy of Sciences, Guangzhou 510070, China

[2] Guangzhou Xinhua University, Guangzhou 510520, China

[3] Southern Marine Science and Engineering Guangdong Laboratory (Guangzhou), Guangzhou 511458, China

[4] State Key Laboratory of Resources and Environmental Information System, Institute of Geographic Sciences and Natural Resources Research, Chinese Academy of Sciences, Beijing 100101, China

‡ Equally contributed to this work

Correspondence: Dan Li (lidan@gdas.ac.cn); Chenghu Zhou (zhouch@lreis.ac.cn)

Abstract. An efficient recognition and extraction of the estuarine turbidity maximum zone (TMZ) is important for studying terrestrial hydrological processes. Although many studies relevant to TMZ have been conducted worldwide, the extraction methods and criteria used to describe TMZ vary significantly both spatially and temporally. To improve the applicability of the methods adopted in previous studies and to develop a

novel model to accurately extract TMZ in multiple estuaries and different seasons from remote sensing imageries, this study estimated the total suspended solids (TSS) and chlorophyll a (Chla) concentrations in three estuaries. These were the Pearl River Estuary (PRE), the Hanjiang River Estuary (HRE), and the Moyangjiang River Estuary (MRE) of Guangdong Province, China. The spatial distribution characteristics of the TSS and Chla concentrations were analyzed. A nearly opposite association was found between the TSS and Chla concentrations in the three estuaries, particularly in the PRE. The regions with high (low) TSS concentrations had relatively low (high) Chla concentrations and therefore, a turbidity maximum zone index (TMZI), defined as the ratio of the difference and sum of the logarithmic transformation of the TSS and Chla concentrations, was firstly proposed. By calculating the TMZI values in the PRE on November 20, 2004 (low-flow season), it was found that the criterion (TMZI > 0.2) could be used to identify the TMZs of the PRE effectively. The TMZ extraction results were generally consistent with the visual interpretation results. The area-based accuracy measures showed that the quality (Q) of the extraction reached 0.8429. The same criterion was applied in the PRE on October 18, 2015 (high-flow season), and high accuracy and consistency across seasons were observed (Q = 0.8171). The western shoal of the PRE was the main distribution area of TMZs. Extracting TMZs by the newly proposed index performed well in different estuaries and on different dates (HRE on August 13, 2008 in the high-flow season and MRE on December 6, 2013 in the low-flow season). Compared to the previous fixed threshold of TSS or turbidity methods,

extracting TMZ using TMZI had higher accuracy and better applicability (Q: 0.1046–0.4770 vs. 0.8171–0.8429). Evidently, this unified TMZI is potentially an optimized method for the global monitoring and extraction of TMZs of estuaries from different satellite remote sensing imageries. It can be used to help the understanding of the spatial and temporal variation of TMZs and estuarine processes at regional and global scales, as well as improve the management and sustainable development of regional society and the natural environment.

Keywords: turbidity maximum zone; turbidity maximum zone index; total suspended solid; chlorophyll a; remote sensing; estuary

1 Introduction

The turbidity maximum zone (TMZ) is the dynamic turbid water area within an estuary, where the suspended solid concentrations, namely, sediment and matter, are consistently and significantly higher than landward and seaward (Shen, 1995; Gebhardt et al., 2005; Yu et al., 2014; Li et al., 2019). It is a special phenomenon of suspended sediment movement and migration in estuaries worldwide (Schubel, 1968; Shi et al., 1993; Mitchell et al., 2012; Wang et al., 2021). The spatial distributions and dynamic changes of TMZs not only have a deep and wide impact on the formation and development of estuary morphology, channels, shoals, and sandbars (Asp et al., 2018; Azhikodan and Yokoyama, 2019; Li et al., 2019), but also significantly affect the physics and geochemical and biogeochemical processes of natural estuarine

environments, as well as social production activities (Gebhardt et al., 2005; Jalón-Rojas et al., 2016; Kitheka et al., 2016; Toublanc et al., 2016; Yan et al., 2020). TMZ has long been a popular area for scientific study and engineering innovations among researchers, government agencies, engineering corporations, and communities (Shen et al., 2001; Shi et al., 2017; Jiang et al., 2019; Wang et al. 2021).

Previous studies have examined TMZ from various aspects based on different data resources and methods, such as the characteristics and dynamics of total suspended solids (TSS) concentrations in TMZ (Yang et al., 2014; Wan and Wang, 2017; Grasso et al., 2018), the mechanisms and formation of TMZ (Brenon and Hir, 1999; Wai et al., 2004; Yu et al., 2014; Toublanc et al., 2016), the location, distribution, and change of TMZ across time (Jiang et al., 2013;Jalón-Rojas et al., 2016; Li et al., 2019; Yan et al., 2020), the interaction with other factors, and its long-term trend (Gebhardt et al., 2005; Chen et al., 2016; Li et al., 2019). The location of TMZ in an estuary is a fundamental question and an important aspect of studying TMZ. It was found that there were two major ways to obtain the locations and distributions of TMZs (Wang et al., 2021). One was a relatively approximate description, such as TMZ locations corresponding to the front of the salinity wedge and moving range of stagnation points, or a distance from coastlines (Feng et al., 2002; Mitchell, 2013; Kitheka et al., 2016; Liu et al., 2016; Toublanc et al., 2016; Gong et al., 2017; Zhang et al., 2019; Yan et al., 2020). The other was a relatively quantitative result. The thresholds of TSS concentrations or turbidity criteria were used to extract the distribution of TMZs (Jiang et al., 2013; Yang and Liu,

84   2015; Chen et al., 2016; Jalón-Rojas et al., 2016; Shi et al., 2017; Li et al., 2019).

85   However, the fixed threshold method has potential drawbacks. It is a challenging task

86   to precisely generate TMZ extraction results at different times using a fixed threshold

87   of TSS concentration because TSS concentrations showed significant variations in

88   different seasons. Moreover, the threshold values are difficult to transfer from local

89   regions to other regions because research and a scientific basis are lacking. The

90   threshold method and criteria vary significantly in different estuaries, in different

91   regions of the same estuary, in the same estuary at different times, and by different

92   studies, demonstrating considerable subjectivity. The results were not comparable

93   (Wang et al., 2021).

94   TSS concentrations in the TMZs and adjacent waters vary significantly (Uncles et

95   al., 2000; Park et al., 2008; Mitchell, 2013; Wang et al., 2018). Many studies have

96   shown that suspended solids can affect the growth of chlorophyll a (Chla) through

97   absorption and sunlight scattering in water (Pozdnyakov et al., 2005; Chen et al., 2015;

98   Montanher et al., 2014; Wang et al., 2017a; Wang et al., 2020b). Therefore, it was

99   concluded that there is a relationship between TSS concentrations and Chla

100   concentrations and different characteristics in TMZ and normal water bodies in

101   estuaries. This relationship might be used to overcome the drawbacks of previous

102   methods of extracting TMZ and distinguish and recognize TMZ effectively.

103   Based on this analysis, the objectives of this study are to propose a new model

104   with better adaptability and robustness for distinguishing and extracting TMZ in

different estuaries and in different seasons. To achieve this goal, the TSS and Chla

concentrations in the Pearl River Estuary (PRE), Hanjiang River Estuary (HRE), and

Moyangjiang River Estuary (MRE) were first estimated. The different spatial

characteristics were analyzed and compared. Subsequently, the corresponding

relationship and special features of TSS and Chla concentrations were used to develop

a turbidity maximum zone index (TMZI). Finally, the TMZs in these estuaries were

extracted at different times by the model (TMZI) and validated and assessed for

accuracy.

The remainder of this paper is organized as follows. The study areas, in situ data,

satellite imagery, TSS concentration data, Chla retrieval model, and its calibration and

validation are described in Section 2, as well as the TMZ extraction accuracy

assessment measures. The spatial analysis of TSS concentration, Chla concentration,

and the corresponding relationship between them are presented in Section 3.1. The

establishment of TMZI and its application and assessment in different estuaries and at

different times are shown in Sections 3.2-3.5. The summary and conclusions are

presented in Section 4.

2 Dataset and methods

2.1 Study areas

The study areas include the Pearl, Hanjiang, and Moyangjiang River Estuaries of

Guangdong Province, South China (Figs. 1, 4, and 7-10). The PRE (horn-shaped) is

located between longitudes 113.45 °–114.2 °E and latitudes 22.25 °–22.85 °N, mainly in

the core zone of Guangdong-Hong Kong-Marco Greater Bay Area. The HRE (forking-

shaped) is located between longitudes 116.6 °–117 °E and latitudes 23.2 °–23.6 °N, mainly

in Shantou city, Eastern Guangdong Province. The MRE (calabash-shaped) is located

between longitudes 111.9 °–112.3 °E and latitudes 21.66 °–21.8 °N, mainly in Yangjiang

city, Western Guangdong Province.
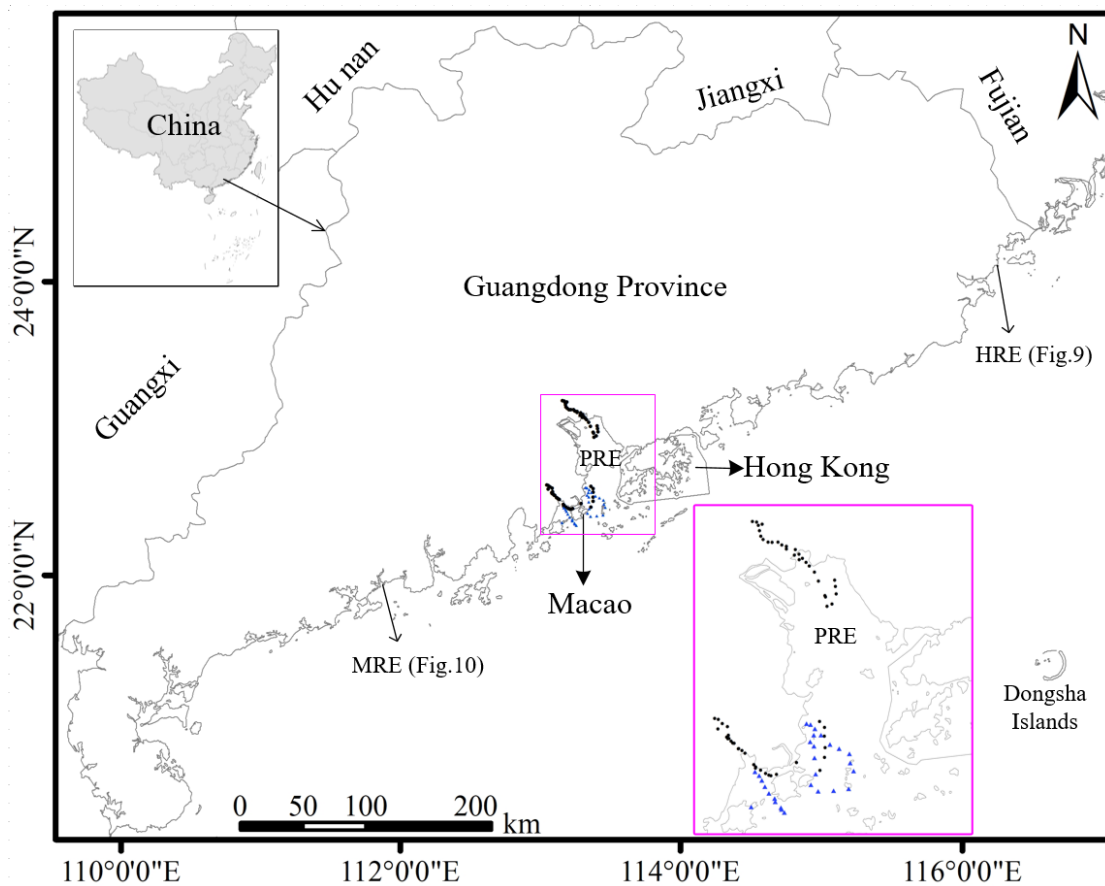
Fig. 1. Study areas (PRE, HRE, and MRE) and the locations of the in-situ data indicated by black

dots and blue triangles.

The Pearl River has the second largest annual runoff and is the third largest river

in China. The Hanjiang and Moyangjiang Rivers are the second and third largest rivers

in Guangdong Province (Chen et al., 2011; Wang et al., 2018; Wang et al., 2020a).

137 Previous studies have reported that the sediment loads of the Pearl, Hanjing and

138 Moyangjiang Rivers were $7.53 \cdot 10^7$, $6.93 \cdot 10^6$ and $3.27 \cdot 10^5$ ton per year, respectively

139 (Wang et al., 2017a, b; Wang et al., 2020a). It was found that the three rivers and

140 estuaries have different characteristics, and much associated research has been

141 conducted in these regions for a long time.

142 2.2 In-situ and satellite data

143 The 89 in-situ samples, including water surface reflectance and Chla

144 concentrations, were collected from the PRE (Fig. 1, Table 1). Sixty of these samples

145 were also used in a previous study by the current authors (black dots) (Chen et al., 2011).

146 The present study included 29 new samples (blue triangles). Here, these samples were

147 used to recalibrate and validate a Landsat-based Chla concentration retrieval model.

148 In addition, four scenes of good quality Landsat imageries were used. Two images

149 from TM and OLI (path/row = 122/44) were captured on November 20, 2004

150 (ProductID: LT05_L1TP_122044_20041120_20161129_01_T1), and October 18,

151 2015 (LC08_L1TP_122044_20151018_20170403_01_T1), respectively, covering the

152 PRE (Figs. 7a and 8c). The image from TM (path/row = 120/44) was captured on

153 August 13, 2008 (LT05_L1TP_120044_20080813_20161030_01_T1), covering the

154 HRE (Fig. 9c). The final image from OLI (path/row = 123/45), was captured on

155 December 6, 2013 (LC08_L1TP_123045_20131206_20170428_01_T1), covering the

156 MRE (Fig. 10c).

157 **Table 1**

158 The 89 in-situ data.

Date	Samples	Measurements	
Dec 9, 2006	16	Reflectance, Chla	
Dec 21, 2006	12	Reflectance, Chla	Same as
Dec 27, 2007	15	Reflectance, Chla	Chen et al. (2011)
Dec 31, 2007	17	Reflectance, Chla	
Nov 2, 2012	18	Reflectance, Chla	
Sep 10, 2013	11	Reflectance, Chla	Newly added

159
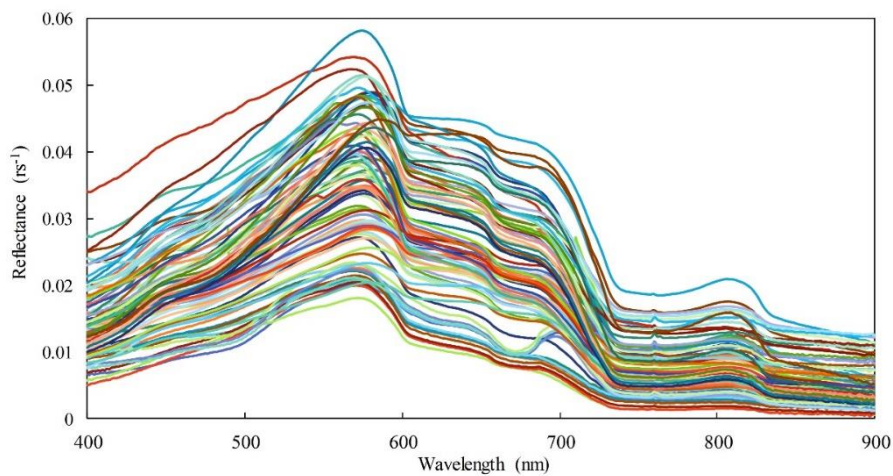
160

161 **Fig. 2.** Remote sensing reflectance of surface water of the 89 in situ data.

162 ## 2.3 Total suspended solids data and chlorophyll a data

163   The aim of this study was to establish and develop a new model (TMZI) based on

164 TSS concentrations and Chla concentrations, and further extract TMZs in three

165 estuaries of Guangdong Province. Therefore, the TSS and Chla concentrations in the

166 study areas were first calculated. The TSS concentration data were obtained from

167 previous work of the current authors (Wang et al., 2017a, b; Wang et al., 2018; Wang et

168 al., 2020a). The corresponding Chla data required retrieval using Landsat imagery.

169 Consequently, a Landsat-based Chla concentration retrieval model was expected to be

170 suitable for different estuaries. Many models have been developed to estimate Chla

171 concentration from different remote sensing data (Gregg and Casey, 2004; Chen et al.,

172 2011; Kim et al., 2016a, b; Attila et al., 2018). Following the features and forms of

173 some typical chlorophyll a retrieval models (Le et al., 2009; Chen et al., 2011; Le et al.,

174 2013; Song et al., 2013), a three-band Landsat-based chlorophyll a model using the 89

175 in-situ samples was recalibrated and validated (Fig. 3; Equation 1). The model, based

176 on Landsat TM and OLI sensors, explained approximately 80% of the Chla

177 concentration variation (Chla: 1.92-92.6 mg/m^3, N=60, P-value<0.01) and had an

178 acceptable validation accuracy (Chla: 2.33-36.8 mg/m^3, RMSE≤3.76 mg/m^3, N=29).
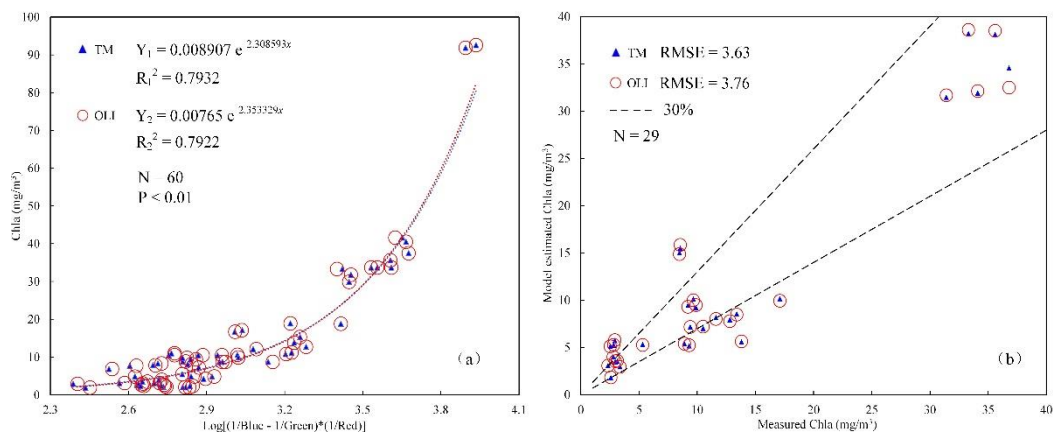
180 **Fig. 3.** The calibration (a) and validation (b) results of the Chla retrieval models based on 89 in situ

181 data for Landsat sensors.

182

$$Chla = a * e^{b*Log_{(10)}[(\frac{1}{R_1} - \frac{1}{R_2}) * \frac{1}{R_3}]}$$ (1)

183   where R_1, R_2 and R_3 represent the blue, green, and red band of theTM and OLI

184   sensors, respectively. The parameters a and b corresponding to the TM and OLI sensors

185   are 0.008907, 2.308593 and 0.00765, 2.353329, respectively. The unit of chlorophyll a

186   concentration is in mg/m^3.

2.4 Accuracy assessment measures

188   To evaluate TMZI extraction accuracy and compare the performances of the

189   different methods, the common accuracy measures of object recognition in remote

190   sensing, area-based accuracy measures (Cai et al., 2018), was used.

191   Suppose that A_E is the area of the extracted TMZ, A_C is the correct part of A_E, and

192   A_R is the reference TMZ. Then the quality (Q) of the TMZ extraction results in the study

193   could be defined as follows (equation 2).

$$Q = \frac{A_C}{A_E + A_R - A_C}$$ (2)

195   The range of Q is 0 to 1. The bigger the Q value, the higher the accuracy of the

196   TMZ extraction results, and the better performance of the method.

3 Results and discussion

3.1 The spatial characteristics of TSS and Chla concentrations in estuaries

200   Chla concentrations in each estuary were estimated using the Chla concentration

201   retrieval model that was developed (Fig. 3). The different spatial distribution

202   characteristics of the TSS and Chla concentrations were analyzed. Taking the PRE as

203 an example, TSS concentrations in the low-flow season of the PRE (November 20,

204 2004) have a large variation ranging from 1.37 mg/L to more than 200 mg/L (Fig. 4a).

205 Due to the strong interaction between runoff and tide, the main region of high TSS

206 concentrations is in the west shoal of the PRE (Wang et al., 2018), where concentrations

207 of more than 100 mg/L were frequently found. In addition, TSS concentrations in parts

208 of the east shoal and Neilingding island adjacent waters were also relatively higher. The

209 other areas of the PRE have low TSS concentrations, where the maximum value is

210 generally not more than 40 mg/L, particularly in the Hong Kong coastal water bodies

211 (Fig. 4a).
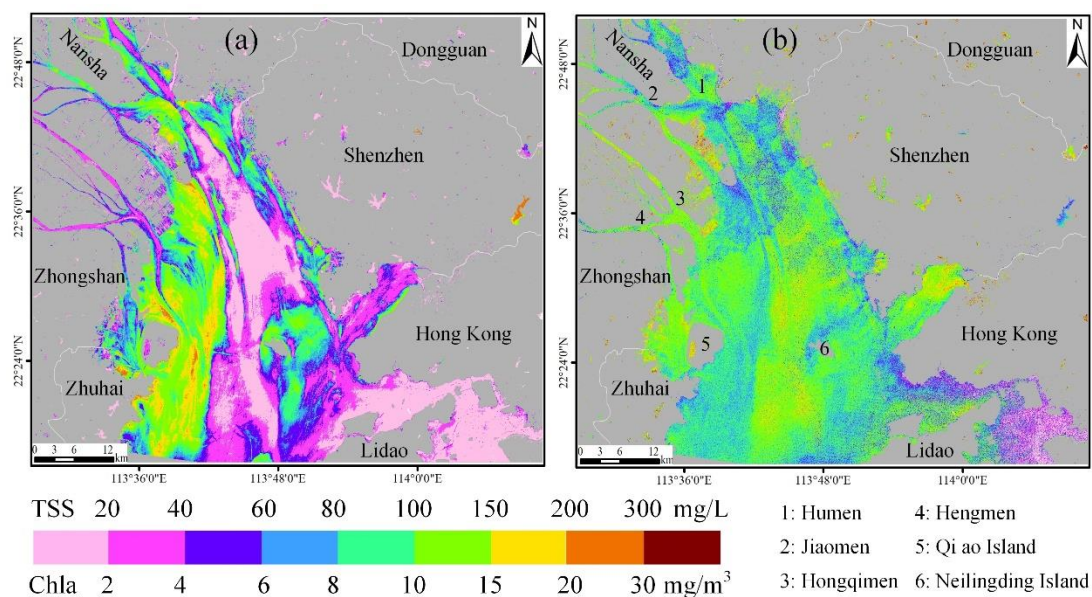
212

213 **Fig. 4.** The estimated TSS concentrations (a) and Chla concentrations (b) in the PRE on November

214 20, 2004.

215   In contrast to the TSS concentration results, the Chla concentrations in the PRE

216 have significantly lower values of less than 20 mg/m^3 in almost the entire PRE (Fig.

217 4b). The results concord with the findings of Liu et al. (2017) and Huang et al. (2005),

218   who found that Chla concentrations ranged from 0.24 mg/m^3 to 21.5 mg/m^3 in the PRE

219   at different times. Furthermore, Chla concentrations in the PRE show almost opposite

220   spatial characteristics to TSS concentrations. Apart from the eastern Lidao district

221   coastal water bodies, the regions of relatively high (low) Chla concentrations are the

222   regions of relatively low (high) TSS concentrations. These corresponding features are

223   apparent in the four waterways, namely, Humen, Jiaomen, Hongqimen, and Hengmen

224   waterways and the shoals, and channels of the PRE (Fig. 4).

225   To further analyze and assess the corresponding relationship between TSS and

226   Chla concentrations in the estuaries, three rows of TSS and Chla concentration values

227   in the PRE were extracted (Fig. 7a; pink lines; rows 1200, 1600, and 1900, columns

228   from 800 to 1300). The results for row 1600 are shown in Fig. 5(a). A correlation

229   analysis showed a significant negative correlation between TSS and Chla

230   concentrations. For the original TSS and Chla concentrations, the correlation

231   coefficient was -0.6531. The correlation coefficient reaches approximately -0.9 for its

232   trend lines (Fig. 5a).

233   3.2 Establishment and application of TMZI

234   Based on the analysis and corresponding features between TSS and Chla

235   concentrations, it is considered that the transform results derived from the two water

236   color elements may help to better distinguish and extract TMZ. In this study, TMZI was

237   defined as the ratio of the difference and sum of logarithmic transformation of TSS

238 concentrations and Chla concentrations (equation 3), which is similar to the normalized

239 difference vegetation index (NDVI).

240 $$TMZI \; = \; [Log(TSS) - Log(Chla)] \; / \; [Log(TSS) + Log(Chla)] \qquad (3)$$
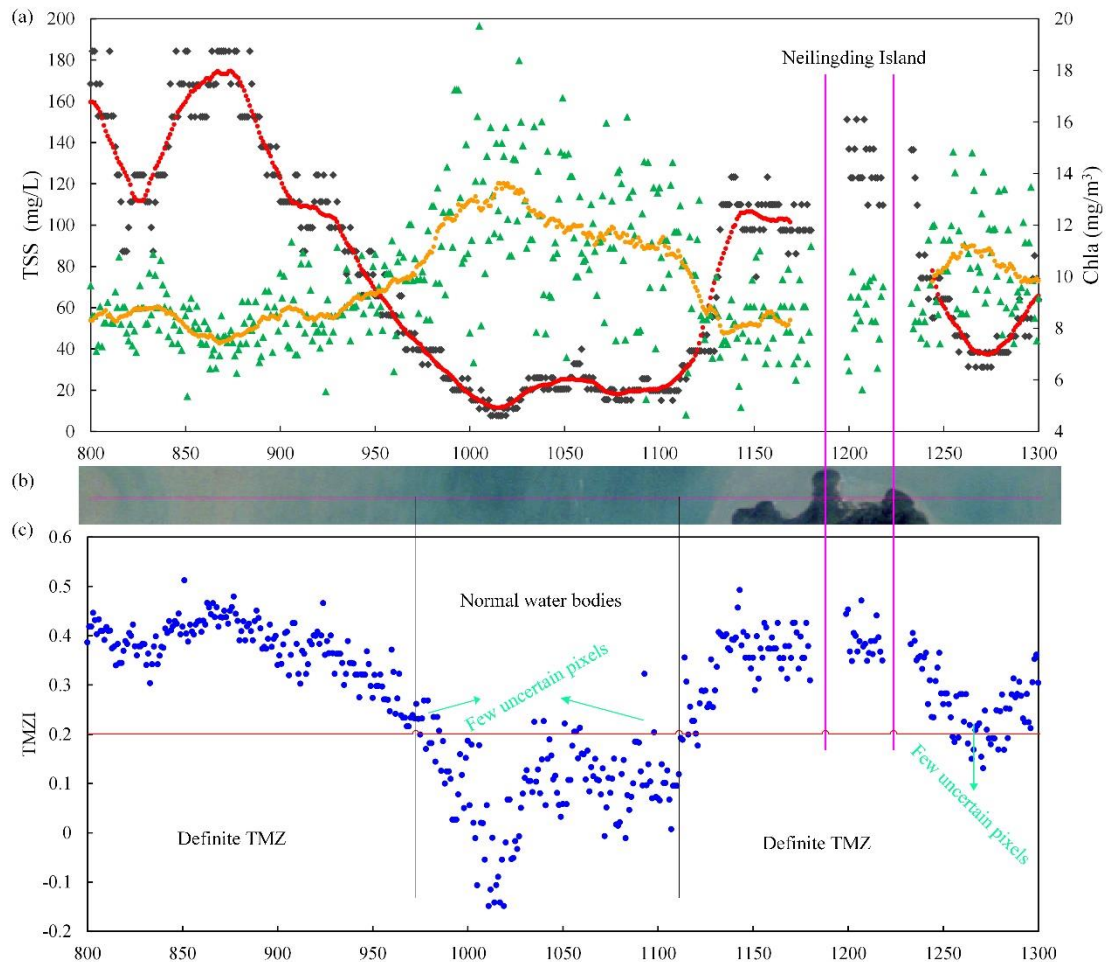
Fig. 5. The corresponding spatial relationship between the TSS concentrations, indicated by black

dots and red trend line, and Chla concentrations, indicated by green triangles and orange trend line

of row 1600 (a), the true color imagery (b) and the corresponding values of TMZI (c).

According to the definition and equation, this study calculated TMZI values (Figs.

5c, 6b and d). Taking the results of row 1600 as an example (Fig. 5b and c), the row

pixels can be mainly divided into one TMZ (columns 800-975), normal water bodies

(columns 975-1110), and another TMZ (columns 1110-1300) from left to right. The null

249 values located in columns 1180-1200 and 1220-1235 are Neilingding Island (Figs. 5

250 and 7a). Through a comparison with the results of TMZI, it is found that all the values

251 of TMZI corresponding to TMZ pixels are larger than 0.2, while the values

252 corresponding to normal water body pixels are all smaller than 0.2, except for a few

253 blurry pixels (Figs. 5b and c). For the results of rows 1200 and 1900, similar

254 corresponding characteristics between TMZ and TMZI and the same criterion were also

255 found (Fig. 6). Therefore, TMZI showed a significant feature and had the potential to

256 develop into a better model for recognizing and extracting estuarine TMZ.
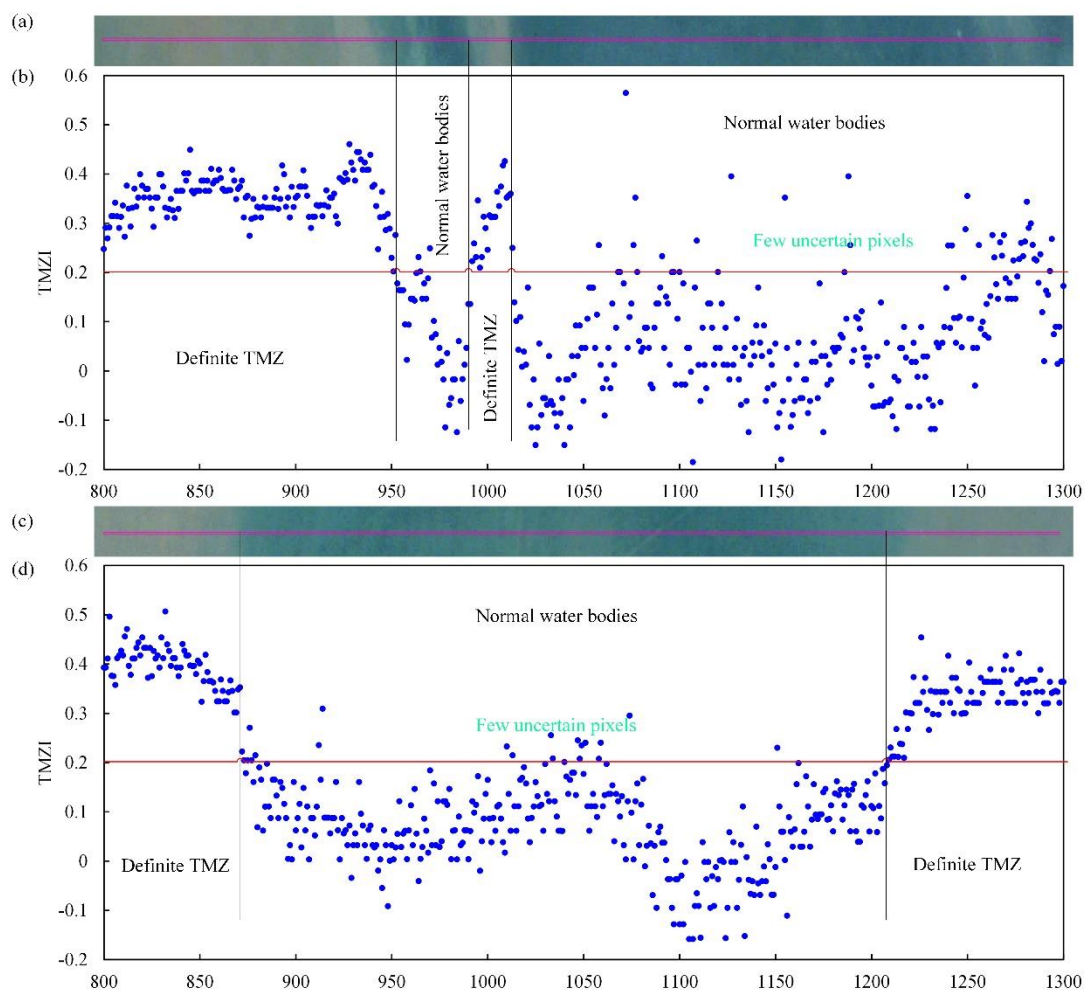
257

258 **Fig. 6.** The true color imagery and the corresponding values of TMZI of rows 1200 (a and b) and

259 1900 (c and d).

The TMZI of the entire Landsat TM imagery was subsequently calculated, and TMZs in the PRE were extracted. Fig. 7(b) shows the spatial distribution results of TMZ in the PRE on November 20, 2004. TMZ is widely distributed throughout the PRE, accounting for more than half of the water areas in the imagery. Among them, the main TMZ is located within an average distance of 11 km from the Panyu, Nansha, Zhongshang, and Zhuhai coasts, which approximately corresponds to the west shoal in the PRE. In the western Dongguan and Shenzhen coastal water bodies, an approximately rectangular TMZ develops approximately 5 km from the coastline, which indicates the location of the east shoal of the PRE (Wang et al., 2018). In addition, a third main TMZ in the PRE located from surrounding Neilingding Island to western Hong Kong water bodies is found, although TSS concentrations in TMZ are lower than those of the former TMZs (Figs.4a and 7b). Compared to the visual interpretation of TMZ results in previous works by the current authors (Fig.7 a) (Wang et al., 2020b, 2021), the area-based accuracy measures show that the quality of extraction achieves 0.8429. The good TMZ extraction results and the high validation accuracy by TMZI in this study indicate a more effective way to recognize TMZs in estuaries (Figs. 6-7).

276
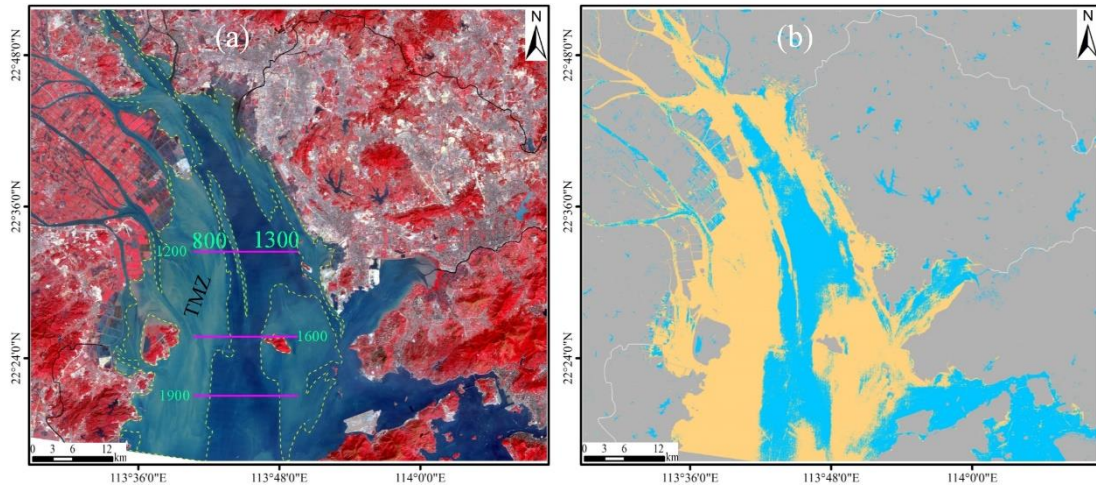
Fig. 7. False color imagery (USGS 1982; NASA 2001) and the visual interpretation TMZ results

(regions indicated by yellow dashed frames) (Wang et al., 2020b, 2021) (a), and the extracted TMZ

results, indicated by mango colors (b) in the PRE on November 20, 2004 (low-flow season).

3.3 Validation of the accuracy of TMZI in different seasons

Due to the complexity of hydrodynamic environments, the estuarine factors and

water color elements show significant variations in different seasons, even in the same

estuary at different times of the day. Therefore, this study further validated the accuracy

of TMZI for extracting TMZ in the PRE during the high-flow season (October 18, 2015).

Fig. 8(a) and (b) demonstrate the retrieved TSS and Chla concentration results in

the high-flow season of PRE. The results in different seasons are significantly different

(Figs. 4 and 8). On October 18, 2015, TSS concentrations in the PRE had wider

variables, ranging from 2.23 to 286.6 mg/L. However, the water bodies with high TSS

concentrations (more than 80 mg/L) were mainly in the outlets of four waterways,

namely, the Humen, Jiaomen, Hongqimen, and Hengmen waterways. The other regions

of the PRE have significantly lower TSS concentrations of generally less than 20 mg/L (Fig. 8a). Similar to the corresponding features between TSS and Chla concentrations in the low-flow season, the almost opposite spatial characteristics remain in the high-flow season. For regions with relatively high (low) Chla concentrations there are relatively low (high) TSS concentrations (Figs. 8a and b). Notably, the eastern Lidao district coastal water bodies are an exception, with the same results in the low-flow season (Fig. 4). Both TSS and Chla concentrations in the zone are relatively low (Figs. 4 and 8).
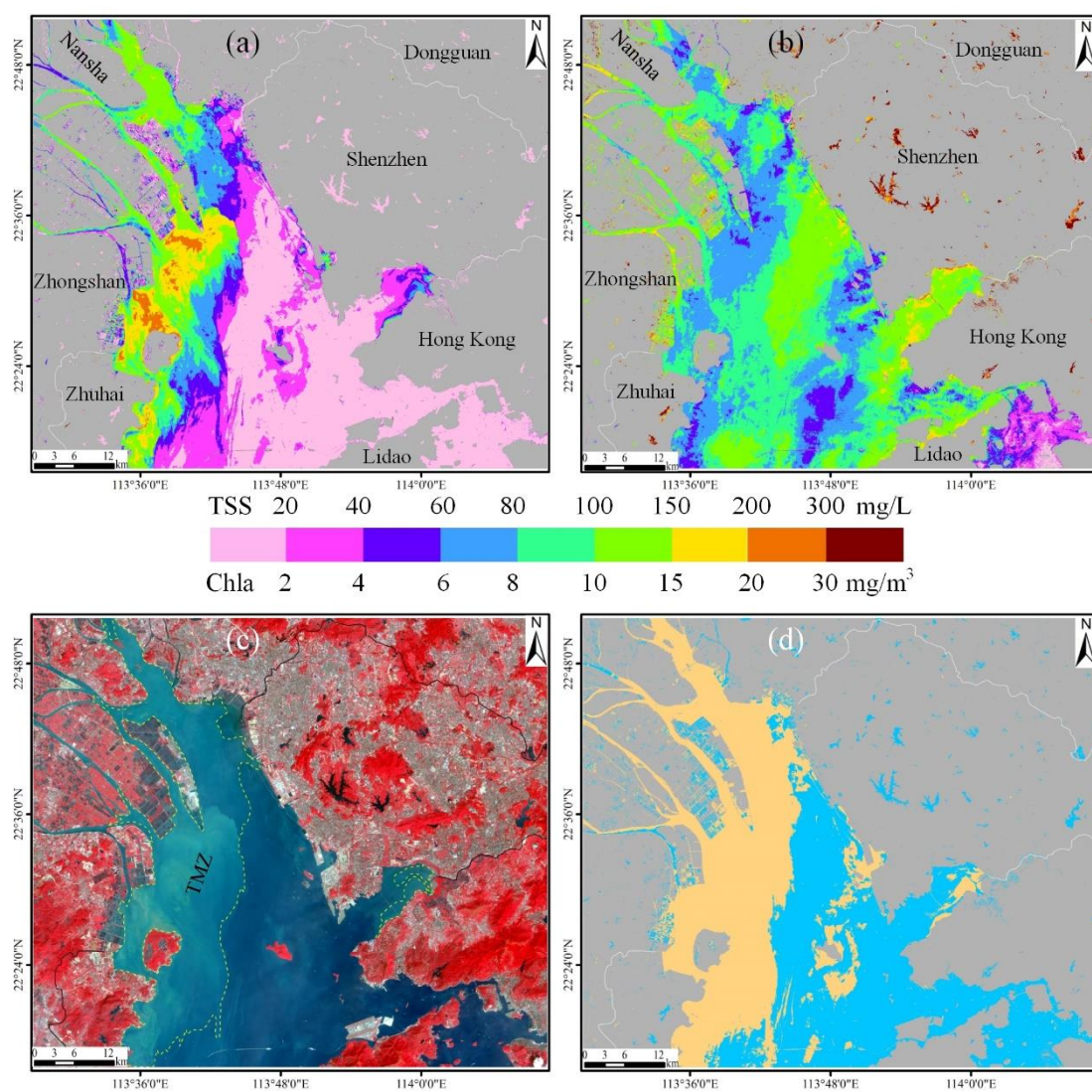
Fig. 8. The estimated TSS concentrations (a), Chla concentrations (b), false color imagery (USGS 1982; NASA 2001), and the visual interpretation TMZ results (regions indicated by yellow dashed frames) (Wang et al., 2020b) (c), and extracted TMZ results, indicated by mango colors mango colors (d) in the PRE on October 18, 2015 (high-flow season).

Using the results of TSS and Chla concentrations of the PRE on October 18, 2015, the TMZI was calculated and TMZs of the PRE were extracted in the high-flow season (Fig. 8d). Compared with the visual interpretation TMZ results (Fig.8 c) (Wang et al., 2020b), the area-based accuracy measures show that the quality of extraction is 0.8171. It is also indicated that an acceptable accuracy is obtained by TMZI in the high-flow season of the PRE. In addition, only one main TMZ remains along the west coast of the PRE (Fig. 8d), which is similar to one of the main TMZs in the low-flow season of 2004 (Fig. 7b). However, clear differences remain in different seasons, such as TMZs in the Hongqimen and Hengmen waterways and the eastern Zhuhai coasts (Figs. 7b and 8d). The other TMZs in the high-flow season of 2015 are mainly located in the surrounding Dachanwan Wharf of Shenzhen and Neilingding Island. The distributions are less apparent than those in the low-flow season of 2004 (Fig. 7b). Besides, two relatively small isolated TMZs can be found on the two artificial islands of the Hong Kong-Zhuhai-Macao Bridge (Fig. 8d), which may imply the associated influence of human activities.

3.4 Assessment of the applicability of TMZI in different estuaries

To further assess the applicability of TMZI in different estuaries, as for the PRE, the corresponding TMZ results in the HRE and the MRE were also calculated and validated.
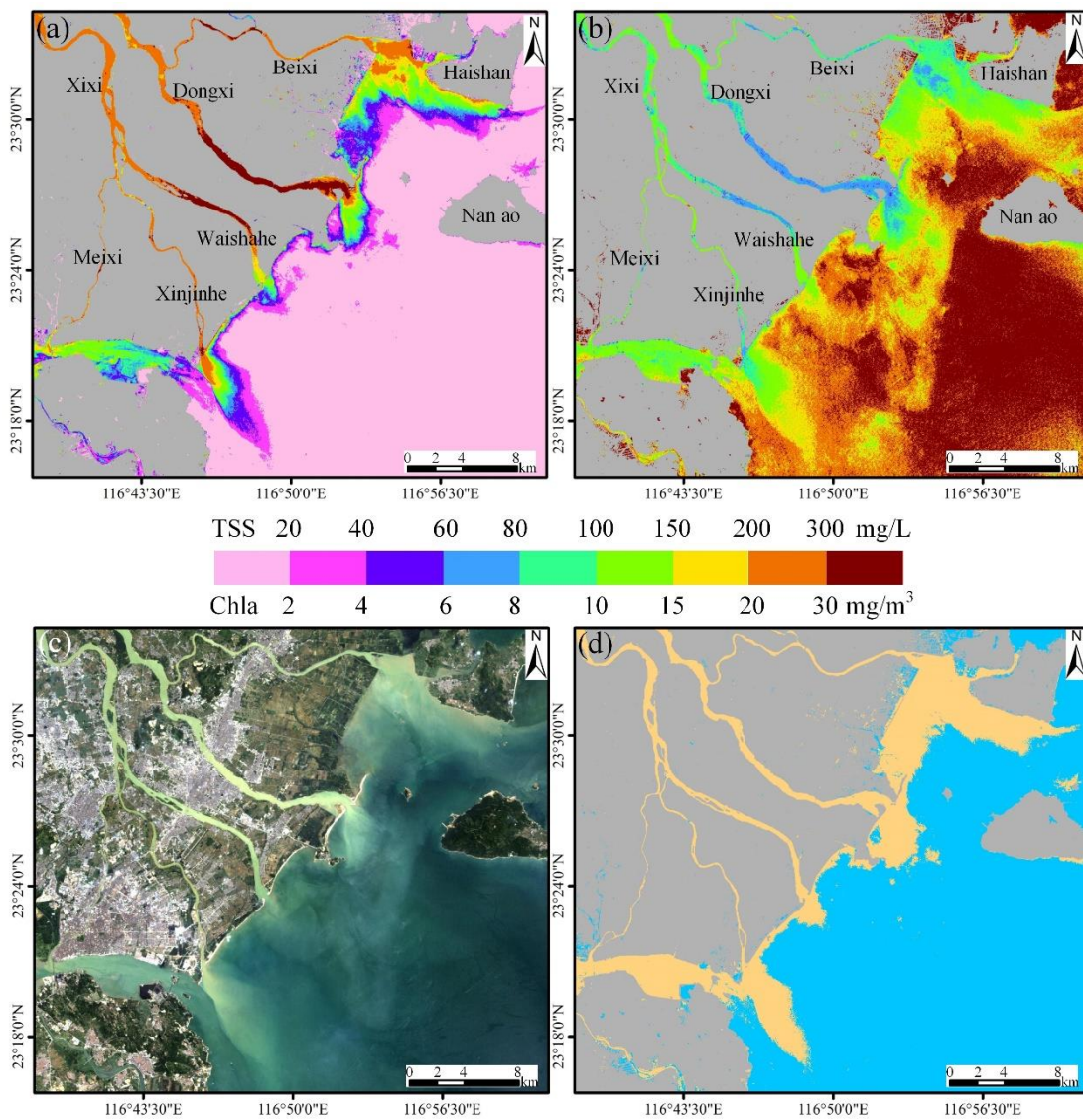
Fig. 9. The estimated TSS concentrations (a), Chla concentrations (b), true color imagery (USGS 1982; NASA 2001) (c), and extracted TMZ results, indicated by mango colors (d) in the HRE on August 13, 2008 (high-flow season).

Fig. 9 (a) and (b) indicate the results of TSS and Chla concentrations in the HRE on August 13, 2008. The TSS concentrations downstream and in the estuary of the HRE are significantly higher than the outer shelf area, particularly in the downstream of the Dongxi River and Xinjinhe River waterways of the Hanjiang River, with a mean value in excess of 300 mg/L (Fig. 9a). TSS concentrations in the offshore area (South China Sea) are frequently less than 20 mg/L. Therefore, a significant decreasing trend of TSS concentration is found from the northwest to southeast in the HRE (Fig. 9a). Furthermore, the Chla concentrations in the HRE show opposite spatial distributions characteristics, which resembles the findings in the PRE (Figs. 4 and 8). Relatively low Chla concentrations are mainly generally found in the downstream and estuary, and the outer shelf area has high values (Fig. 9b). The Chla concentrations in the HRE range from 4.1 to 37.3 mg/m^3 (Fig. 9b), which is slightly higher than that of the PRE (Figs. 4 and 8).

The TMZ extraction results for the HRE are shown in Fig. 9(d). The TMZs are distributed in all the downstream and estuaries of the Hangjiang River. They can be divided into four main TMZs based on different waterways, namely, the Beixi, Dongxi, Waishahe, Xinjinhe, and Meixi waterways of the Hanjing River. The maximum TMZ is located within an average distance of 3 km from the Beixi estuary, western Haishan

coast, and the coastlines between the Beixi and Dongxi estuaries. The second largest

TMZ of the HRE is distributed from the Meixi to the Xinjinhe estuaries. The region of

the main TMZ of the Xinjinhe estuary appears knife-shaped, which is mainly caused

by the runoff of the Xinjinhe waterway and the flow guiding line connected to Longhu

District, Shantou City (Fig. 9 d) (Wang et al., 2017a). The other two relatively smaller

TMZs are distributed in the Dongxi and Waishahe estuaries, respectively. The results

indicate that the TMZ distribution in the HRE is mainly related to tide, runoff, estuarine

topography, and human activity.

In the MRE, the region of high TSS concentrations is mainly distributed at an

average distance of 1.2 km from the Yangjiang coastlines, particularly in the eastern

Hailingdati dike water bodies, with a mean value of more than 150 mg/L (Fig. 10a).

The outer shelf area has significantly lower TSS concentrations of generally less than

35 mg/L. The Chla concentrations in most regions of the MRE are more than 4 mg/m^3,

except for the southwestern Dongping town coastal water bodies, where Chla

concentrations mainly range from 2 to 4 mg/m^3. The Chla concentrations in the

Moyangjiang River downstream, Fuchang town coast, and outside of the Shouchanghe

River estuary have relatively high values of frequently greater than 8 mg/m^3 (Fig. 10b).

Compared to the PRE and the HRE, the corresponding relationship between TSS and

Chla concentrations in the MRE is slightly weak. However, a trend of high (low) TSS

concentrations in water bodies with relatively low (high) Chla concentrations remains

(Figs. 10a and b).
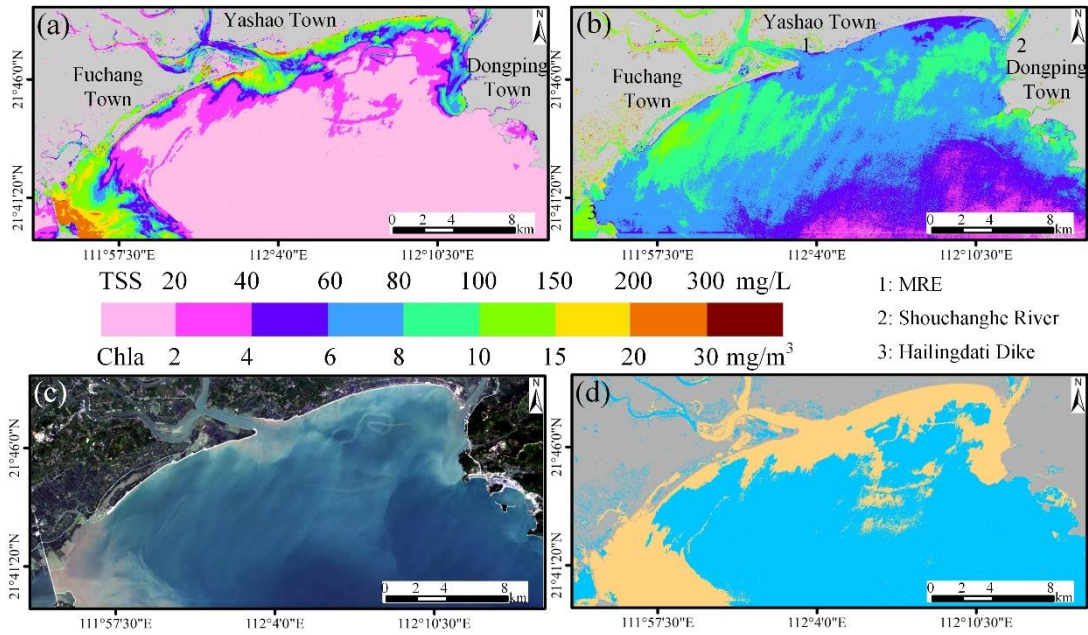
369

370 **Fig. 10.** The estimated TSS concentrations (a), Chla concentrations (b), true color imagery (USGS

371 1982; NASA 2001) (c), and extracted TMZ results, indicated by mango colors (d) in the MRE on

372 December 6, 2013 (Low-flow season).

373   Figs. 10 (c) and (d) indicate the true color imagery of the MRE and the TMZs

374 extraction results. There are two main TMZs in the MRE on December 6, 2013. The

375 first TMZ is mainly distributed from the inside and outside of the Moyangjiang River

376 estuary to the Shouchanghe River estuary, with a distance of approximately 1.8 km

377 from the coastlines (Fig. 10d). The distribution of TMZ in this region is mainly

378 attributed to the interaction of tide and runoff. Another main TMZ is in the regions 4

379 km from the Hailingdati dike, and is mainly caused by obstruction against ocean

380 currents (Fig. 10d). In addition, several small, long, and narrow TMZs are accuracy

381 extracted through TMZI with the same criterion as that in the PRE and the HRE.

The results of the three estuaries and the comparison and accuracy assessment indicate that extracting TMZ based on TMZI and the criterion (TMZI > 0.2) has a high applicability in multiple eatuaries and different seasons.

3.5 Comparison with the previous methods

Previous studies have extracted TMZ based mainly on the threshold of TSS concentrations or turbidity. For example, Jalón-Rojas et al. (2016) used thresholds of 500 mg/L (300 NTU) and 1000 mg/L (600 NTU) to define moderately concentrated TMZ and highly concentrated TMZ in the Loire Estuary in France; Jiang et al. (2013) and Li et al. (2019) defined TMZ as the areas with TSS values larger than 700 mg/L in Yangtze Estuary and Hangzhou Bay. For TMZ in the PRE, it was found that TSS values in studies by Shi et al. (2017) and Wai et al. (2004) were more than 89.4 mg/L and about 150 mg/L, respectively. Based on the two criteria (TMZ: TSS > 89.4 mg/L or TSS > 150 mg/L), this study calculated and extracted TMZs in the PRE (Fig. 11c-f).

Compared to the visual interpretation TMZ results (Figs. 7a and 8c), the TMZ extraction results in the PRE based on the criterion of Shi et al. (2017) are superior to those of Wai et al. (2004), on November 20, 2004 (Fig. 11c vs. Fig. 11e, low-flow season) or October 18, 2015 (Fig. 11d vs. Fig. 11f, high-flow season). The extraction quality based on the criteria of Shi et al. (2017) and Wai et al. (2004) are 0.4238, 0.4770 and 0.1046, 0.1661, respectively. The primary reason may be that the time of the data source in Shi et al. (2017) was closer to the present study than that in the study by Wai

402 et al. (2004). This means that the criterion of Shi et al. (2017) was more suitable for this

403 study than that of Wai et al. (2004).

404
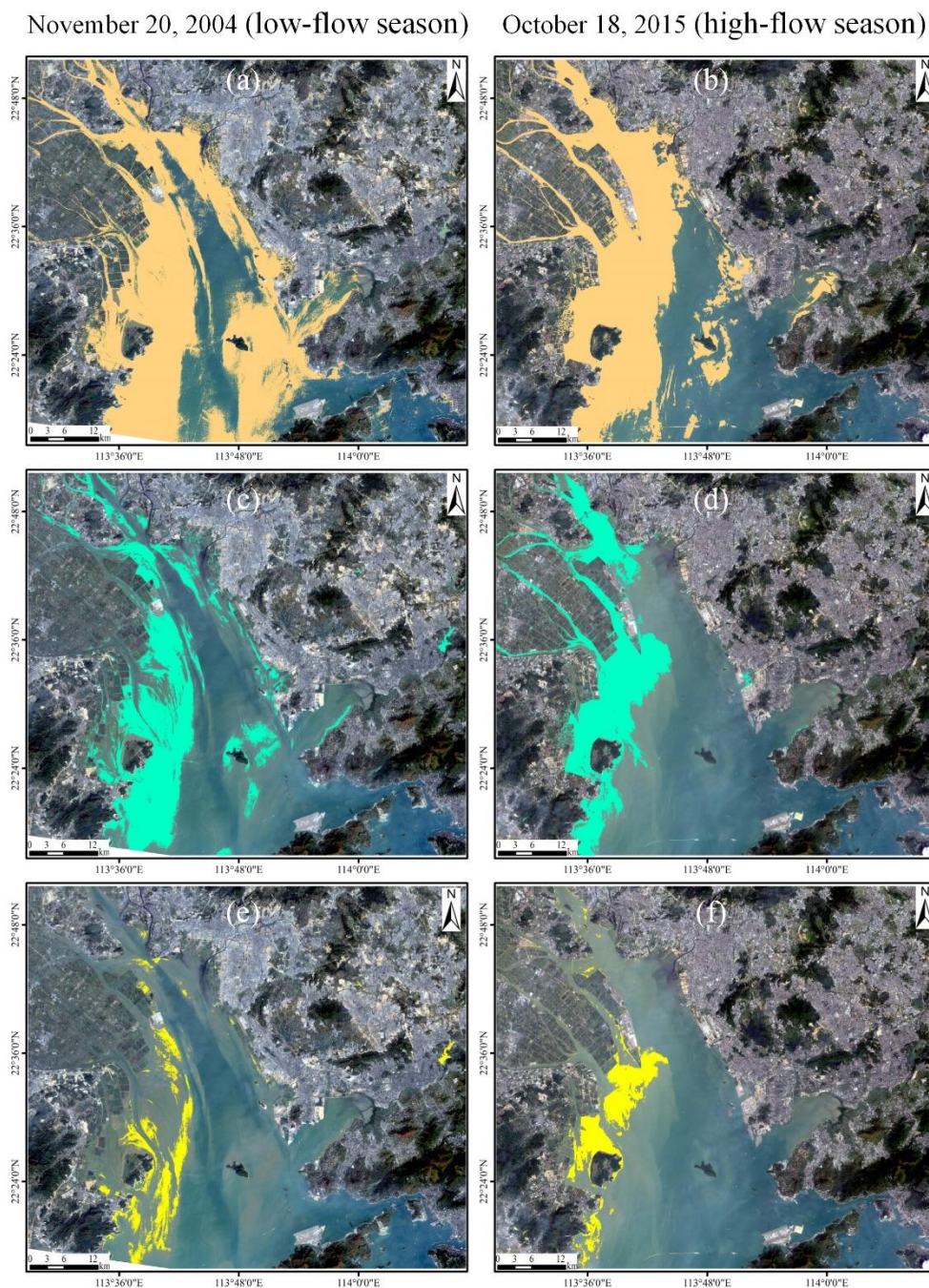
405 **Fig. 11.** The true color imagery (USGS 1982; NASA 2001) and TMZ extraction results in the PRE

406 at different time (a, c, e: November 20, 2004; b, d, f: October 18, 2015) based on the TMZI method

407 of this study (a and b, regions indicated by mango color, as in Fig. 7b and Fig. 8d), the criterion by

408 Shi et al. (2017) (c and d, regions indicated by cyan color), and the criterion by Wai et al. (2004) (e

409 and f, regions indicated by yellow color).

410 It was also found that a relatively good result was obtained in the west shoal of the

411 PRE on November 20, 2004, according to the criterion of Shi et al. (2017) (Fig. 11c).

412 The extracted TMZs are almost consistent with the reality compared to the true color

413 imagery and the visual interpretation TMZ results (Wang et al., 2020b, 2021). However,

414 the accuracy in the east shoal and surrounding Neilingding Island of the PRE is lower

415 than in the west shoal, where obvious distributions of TMZs are not recognized

416 effectively (Fig. 11c). Furthermore, the same criterion does not work well in the western

417 shoal of the PRE at different times (Fig. 11c vs. Fig. 11d). Almost one-third of the

418 distributions of TMZs in the western shoal of the PRE during the high-flow season are

419 not distinguished and extracted (Fig. 11d). The results based on the criteria of previous

420 studies, indicate that fixed thresholds have a distinct disadvantage when extracting

421 TMZ at different times or in estuaries.

422 Based on the evaluation and analysis of all the above results (Figs. 7-11), TMZI

423 could be widely and effectively applied for the accurate extraction of estuarine TMZ,

424 regardless of the significant variations in hydrodynamic environments, TSS and Chla

425 concentrations in different estuaries and seasons. Compared to previous studies and the

426 results from fixed thresholds, it is concluded that TMZI has significant potential to

427 develop into a unified model for distinguishing and extracting TMZ effectively and

428 accurately in many other estuaries globally (Q: 0.8171-0.8429 vs. 0.1046-0.4770).

4 Summary and Conclusions

This study established and developed a novel model (turbidity maximum zone index) based on TSS and Chla concentration, to distinguish estuarine turbidity maximum zone from Landsat imageries. It was found that both TSS and Chla concentrations showed significant variations and different characteristics in the PRE, the HRE and the MRE in different times (Figs. 4 and 8-10). A corresponding relationship between TSS and Chla concentrations in the three estuaries of Guangdong Province remains. In this study, the Chla and TSS concentrations showed almost opposite spatial distribution characteristics, where relatively high (low) Chla concentrations corresponded exactly to the relatively low (high) TSS concentrations (Figs. 4-5 and 8-10). Therefore, here, the turbidity maximum zone index (TMZI) was defined and designed as the ratio of the difference and sum of the logarithmic transformation of TSS and Chla concentrations.

Compared with the true (false) color imagery and the visual interpretation TMZ results, it was found that the TMZ extraction results by TMZI were consistent with the reality (Figs. 7-10; Q: 0.8171-0.8429). Notably, the criterion used for extracting TMZs in different estuaries and seasons was the same (TMZI > 0.2). In addition, reasonable accuracy and a better performance were obtained by TMZI compared with the previous fixed TSS concentration or turbidity threshold (Fig. 11; Q: 0.8171-0.8429 vs. 0.1046-0.4770), demonstrating that TMZI has a higher adaptability and robustness.

449   The results of this study indicate that there is significant potential for optimizing

450   TMZI to distinguish and extract TMZs from multi-source satellite remote sensing, such

451   as Sentinel, Aqua & Terra-MODIS, Envisat MERIS and SeaWiFS. This will also assist

452   in establishing and developing a global unified criterion for extracting TMZs effectively

453   in different estuaries and at different times.

454   **Code and data availability**

455   All the Landsat remote sensing imageries are fully available at

456   https://glovis.usgs.gov/ (USGS 1982; NASA 2001).

457   **Author Contribution**

458   The individual contributions and responsibilities of the authors are listed as

459   follows: Chongyang Wang and Li Wang designed the research and wrote the paper;

460   Chenghu Zhou and Dan Li guided the research process; Danni Wang, Qiong Zheng,

461   Hao Jiang, Kai Jia and Yangxiaoyue Liu collected and analyzed the data; Shuisen Chen,

462   Ji Yang, Xia Zhou and Yong Li revised the manuscript, provided some comments and

463   helped edit the manuscript. All authors have read and agreed to the published version

464   of the manuscript.

465   **Competing interests**

466   The authors declare that they have no conflict of interest.

Acknowledgements

This work was funded jointly by National Natural Science Foundation of China (41801364), Natural Science Foundation of Guangdong Province (2021A1515012579), Key Special Project for Introduced Talents Team of Southern Marine Science and Engineering Guangdong Laboratory (Guangzhou) (GML2019ZD0301), Scientific Research Project approved by Department of Education of Guangdong Province (2019KQNCX209), Guangdong Innovative and Entrepreneurial Research Team Program (2016ZT06D336) and GDAS' Project of Science and Technology Development (2020GDASYL-20200104006, 2020GDASYL-20200302001, 2019GDASYL-0503001, 2019GDASYL-0301001 and 2019GDASYL-0501001). We would also like to thank USGS for providing the Landsat remote sensing imageries.

References

Asp, N.E., Gomes, V., Schettini, C.A.F., Filho, P.W.S., Siegle, E., Ogston, A.s., Nittrouer, C.A., Silva, J.N.S., Nascimento, W.R., Jr, Souza, S.R., Pereira, L.C.C., Queiroz, M.C., 2018. Sediment dynamics of a tropical tide-dominated estuary: Turbidity maximum, mangroves and the role of the Amazon River sediment load. Estuarine, Coastal and Shelf Science.

Attila, J., Kauppila, P., Kallio, K.Y., Alasalmi, H., Keto, V., Bruun, E., Koponen, S., 2018. Applicability of Earth Observation chlorophyll-a data in assessment of

486   water status via MERIS-With implications for the use of OLCI sensor. Remote

487   Sensing of Environment. 212, 273-287.

488   Azhikodan, G., Yokoyama, K., 2019. Seasonal morphodynamic evolution in a

489   meandering channel of a macrotidal estuary. Science of the Total Environment.

490   684, 281-295.

491   Brenon, I., Hir, P.L., 1999. Modelling the Turbidity Maximum in the Seine Estuary

492   (France): Identification of Formation Processes. Estuarine, Coastal and Shelf

493   Science. 49, 525-544.

494   Cai, L., Shi, W., Miao, Z., & Hao, M. (2018). Accuracy Assessment Measures for

495   Object Extraction from Remote Sensing Images. Remote Sensing, 10, 303.

496   Chen, S., Fang, L., Li, H., Chen, W., Huang, W., 2011. Evaluation of a three-band

497   model for estimating chlorophyll-a concentration in tidal reaches of the Pearl River

498   Estuary, China. ISPRS Journal of Photogrammetry and Remote Sensing. 68, 356-

499   364.

500   Chen, S., Han, L., Chen, X., Li, D., Sun, L., Li, Y., 2015. Estimating wide range Total

501   Suspended Solids concentrations from MODIS 250-m imageries: An improved

502   method. ISPRS Journal of Photogrammetry and Remote Sensing. 99, 58-69.

503   Chen, X., Shen, Z., Yang, Y., 2016. Response of the turbidity maximum zone in the

504   Yangtze River Estuary due to human activities during the dry season.

505   Environmental Science and Pollution Research. 11, 1-16.

506 Feng, H., Cochran, J.K., Hirschberg, D.J., 2002. Transport and sources of metal

507   contaminants over the course of tidal cycle in the turbidity maximum zone of the

508   Hudson River estuary. Water Research. 36, 733-743.

509 Gebhardt, A.C., Schoster, F., Gaye-Haake, B., Beeskow, B., Rachold, V., Unger, D.,

510   Ittekkot, V., 2005. The turbidity maximum zone of the Yenisei River (Siberia) and

511   its impact on organic and inorganic proxies. Estuarine, Coastal and Shelf Science.

512   65, 61-73.

513 Gong, S., Gao, A., Lin, J., Zhu, X., Zhang, Y., Hou, Y., 2017. Temporal-spatial

514   distribution and its influencing factors of suspended particulate matters in

515   Minjiang lower reaches and estuary. Journal of Earth Sciences and Evironment.

516   39(6), 826-836.

517 Grasso, F., Verney, R., Hir, P.L., Thouvenin, B., Schulz, E., Kervella, Y., Fard, I.K.P.,

518   Lemoine, J.-P., Dumas, F., Garnie, V., 2018. Suspended Sediment Dynamics in the

519   Macrotidal Seine Estuary (France) - Part 1: Numerical Modeling of Turbidity

520   Maximum Dynamics. Journal of Geophysical Research: Oceans. 123, 558-577.

521 Gregg, W.W., Casey, N.W., 2004. Global and regional evaluation of the SeaWiFS

522   chlorophyll data set. Remote Sensing of Environment. 93, 463-479.

523 Huang, B., Hong, H., Ke, L., Cao, Z., 2005. Size-fractionated phytoplankton biomass

524   and productivity in the Zhujiang River Estuary in China. Acta Oceanologica Sinica.

525   27, 180-186.

526 Jalón-Rojas, I., Schmidt, S., Sottolichio, A., Bertier, C., 2016. Tracking the turbidity

527   maximum zone in the Loire Estuary (France) based on a long-term, high-

528   resolution and high-frequency monitoring network. Continental Shelf Research.

529   117, 1-11.

530 Jiang, J., He, Q., Zhu, L., Lin, J., 2019. Analysis of hydrodynamic features of the North

531   Passage in the turbidity maximum, Changjinag Estuary. Haiyang Xuebo. 41(1),

532   11-20.

533 Jiang, X., Lu, B., He, Y., 2013. Response of the turbidity maximum zone to fluctuations

534   in sediment discharge from river to estuary in the Changjiang Estuary (China).

535   Estuarine, Coastal and Shelf Science. 131, 24-30.

536 Kim, H.H., Ko, B.C., Nam, J.Y., 2016a. Predicting chlorophyll-a using Landsat 8 OLI

537   sensor data and the non-linear RANSAC method –a case study of Nakdong River,

538   South Korea. International Journal of Remote Sensing. 37, 3255-3271.

539 Kim, W., Moon, J.-E., Park, Y.-J., Ishizaka, J., 2016b. Evaluation of chlorophyll

540   retrievals from Geostationary Ocean Color Imager (GOCI) for the North-East

541   Asian region. Remote Sensing of Environment. 184, 482-495.

542 Kitheka, J.U., Mavuti, K.M., Nthenge, P., Obiero, M., 2016. The turbidity maximum

543   zone in a shallow, well-flushed Sabaki estuary in Kenya. Journal of Sea Research.

544   110, 17-28.

545   Le, C., Hu, C., Cannizzaro, J., English, D., Muller-Karger, F., Lee, Z., 2013. Evaluation

546   of chlorophyll-a remote sensing algorithms for an optically complex estuary.

547   Remote Sensing of Environment. 129, 75-89.

548   Le, C., Li, Y., Zha, Y., Sun, D., Huang, C., Lu, H., 2009. A four-band semi-analytical

549   model for estimating chlorophyll a in highly turbid lakes: The case of Taihu Lake,

550   China. Remote Sensing of Environment. 113, 1175-1182.

551   Li, L., Ye, T., Wang, X., Xia, Y., 2019. Tracking the multidecadal variability of the

552   surface turbidity maximum zone in Hangzhou Bay, China. International Journal of

553   Remote Sensing. 1-22.

554   Liu, H., Huang, L., Tan, Y., Ke, Z., Liu, J., Zhao, C., Wang, J., 2017. Seasonal variations

555   of chlorophyll a and primary production and their influencing factors in the Pearl

556   River Estuary. Journal of Tropical Oceanography. 36, 81-91.

557   Liu, R., Wang, Y., Gao, J., Wu, Z., Guan, W., 2016. Turbidity maximum formation and

558   its seasonal variations in the Zhujiang (Pearl River) Estuary, southern China. Acta

559   Oceanologica Sinica. 35, 22-31.

560   Mitchell, S., 2013. Turbidity maxima in four macrotidal estuaries. Ocean & Coastal

561   Management. 79, 62-69.

562   Mitchell, S., Akesson, L., Uncles, R., 2012. Observations of turbidity in the Thames

563   Estuary, United Kingdom. Water and Environment Journal. 26, 511-520.

564   Montanher, O., Novo, E., Barbosa, C., Renno, C., Silva, T., 2014. Empirical models for

565   estimating the suspended sediment concentration in Amazonian white water rivers

566   using Landsat 5/TM. International Journal of Applied Earth Observation and

567   Geoinformation, 29, 67-77.

568   Park, K., Wang, H.V., Kim, S.-C., Oh, J.-H., 2008. A Model Study of the Estuarine

569   Turbidity Maximum along the Main Channel of the Upper Chesapeake Bay.

570   Estuaries and Coasts. 31, 115-133.

571   Pozdnyakov, D., Shuchman, R., Korosov, A., Hatt, C., 2005. Operational algorithm for

572   the retrieval of water quality in the Great Lakes. Remote Sensing of Environment.

573   97, 352-370.

574   Schubel, J., 1968. Turbidity maximum of the northern chesapeake bay. SCIENCE. 161,

575   1013-1015.

576   Shen, H., 1995. New understanding on the study of the maximum turbidity zone in

577   estuaries of China. Advence in Earth Sciences. 10, 210-212.

578   Shen, H., He, S., Mao, Z., Li, J., 2001. On the turbidity maximum in the Chinese

579   estuaries. Journal of Sediment Research. 1, 23-29.

580   Shi, W., Shen, H., Li, J., 1993. Review on the formation of estuarine turbidity maximum.

581   Advence in Earth Sciences. 8, 8-13.

582   Shi, Z., Xu, J., Huang, X., Zhang, X., Jiang, Z., Ye, F., Liang, X., 2017. Relationship

583   between nutrients and plankton biomass in the turbidity maximum zone of the

584   Pearl River Estuary. Journal of Environmental Sciences. 57, 72-84.

585   Song, K., Li, L., Tedesco, L.P., Li, S., Duan, H., Liu, D., Hall, B.E., Du, J., Li, Z., Shi,

586   K., Zhao, Y., 2013. Remote estimation of chlorophyll-a in turbid inland waters:

587   Three-band model versus GA-PLS model. Remote Sensing of Environment. 136,

588   342-357.

589   Toublanc, F., Brenon, I., Coulombier, T., 2016. Formation and structure of the turbidity

590   maximum in the macrotidal Charente estuary (France)_ Influence of fluvial and

591   tidal forcing. Estuarine, Coastal and Shelf Science. 169, 1-14.

592   Uncles, R.J., Bloomer, N.J., Frickers, P.E., Griffiths, M.L., Harris, C., Howland, R.J.M.,

593   Morris, A.W., Plummer, D.H., Tappin, A.D., 2000. Seasonal variability of salinity,

594   temperature, turbidity and suspended chlorophyll in the Tweed Estuary. The

595   Science of the Total Environment. 251/252, 115-124.

596   Wai, O.W.H., Wang, C.H., Li, Y.S., Li, X.D., 2004. The formation mechanisms of

597   turbidity maximum in the Pearl River estuary, China. Marine Pollution Bulletin.

598   48, 441-448.

599   Wan, Y., Wang, L., 2017. Numerical investigation of the factors influencing the vertical

600   profiles of current, salinity, and SSC with in a turbidity maximum zone.

601   International Journal of Sediment Research. 32, 20-33.

602   Wang, C., Chen, S., Li, D., Wang, D., liu, W., Yang, J., 2017a. A Landsat-based model

603   for retrieving total suspended solids concentration of estuaries and coasts in China.

604   Geoscientific Model Development. 10, 4347-4365.

605   Wang, C., Chen, S., Yang, J., Li, Y., Zhou, X., Li, D., Wang, D., 2020a. Monitoring total

606   suspended solids concentrations in estuaries based on remote sensing. Beijing:

607   China Water & Power Press.

608   Wang, C., Li, D., Wang, D., Chen, S., 2017b. Detecting the Temporal and Spatial

609   Changes of Suspended Sediment Concentration in Hanjiang River Estuary During

610   the Past 30 Years Using Landsat Imageries. Research Journal of Environmental

611   Science. 11, 143-155.

612   Wang, C., Li, W., Chen, S., Li, D., Wang, D., Liu, J., 2018. The spatial and temporal

613   variation of total suspended solid concentration in Pearl River Estuary during

614   1987–2015 based on remote sensing. Science of the Total Environment. 618, 1125-

615   1138.

616   Wang, C., Wang, D., Yang, J., Fu, S., Li, D., 2020b. Suspended Sediment within

617   Estuaries and along Coasts: A Review of Spatial and Temporal Variations based

618   on Remote Sensing. Journal of Coastal Research. 36, 1323-1331.

619   Wang, C., Zhou, C., Chen, S., Xie, Y., Li, D., Yang, J., Zhou, X., Li, Y., Wang, D., Liu,

620   Y., 2021. Retrospect and perspective of the estuarine turbidity maximum zone

621   researches. Chinese Science Bulletin. 66, 2328-2342.

622   Yan, D., Song, D., Bao, X., 2020. Spring-neap tidal variation and mechanism analysis

623   of the maximum turbidity in the Pearl River Estuary during flood season. Journal

624   of Tropical Oceanography. 39, 20-35.

625   Yang, J., Liu, W., 2015. Characteristics of the maximum turbidity zone in the

626   lingdingyang-Pearl river estuary during the flood season in the recent 30 years.

627   Pearl River Water Transport. 16, 58-62.

628 Yang, Y., Li, Y., Sun, Z., Fan, Y., 2014. Suspended sediment load in the turbidity

629   maximum zone at the Yangtze River Estuary: The trends and causes. Journal of

630   Geographical Sciences. 24, 129-142.

631 Yu, Q., Wang, Y., Gao, J., Gao, S., Flemming, B., 2014. Turbidity maximum formation

632   in a well-mixed macrotidal estuary: The role of tidal pumping. Journal of

633   Geophysical Research: Oceans. 119, 7705-7724.

634 Zhang, X., Chen, X., Dou, X., Zhao, X., Xia, W., Jiao, J., Xu, H., 2019. Study on

635   formation mechanism of turbidity maximum zone and numerical simulations in

636   the macro tidal estuaries. Advances in Water Science. 30, 84-92.